# CO2 binding capacity of alkali-activated fly ash and slag pastes

Nedeljkovic, Marija; Ghiassi, Bahman; Melzer, S; Kooij, Chris; van der Laan, Sieger; Ye, Guang

**DOI**
10.1016/j.ceramint.2018.07.216

**Publication date**
2018

**Document Version**
Accepted author manuscript

**Published in**
Ceramics International

**Citation (APA)**
Nedeljkovic, M., Ghiassi, B., Melzer, S., Kooij, C., van der Laan, S., & Ye, G. (2018). CO2 binding capacity of alkali-activated fly ash and slag pastes. *Ceramics International*, *44*(16), 19646-19660. https://doi.org/10.1016/j.ceramint.2018.07.216

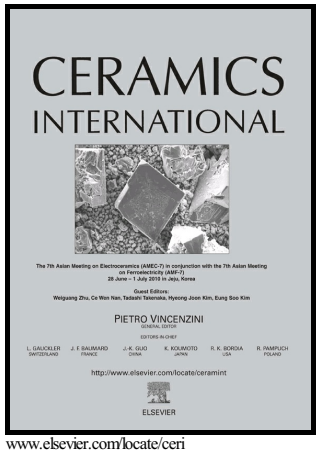


www.elsevier.com/locate/ceri

# $CO_2$ binding capacity of alkali-activated fly ash and slag pastes

Marija Nedeljković, Bahman Ghiassi, Stefan Melzer, Chris Kooij, Sieger van der Laan, Guang Ye

PII: S0272-8842(18)31958-8
DOI: https://doi.org/10.1016/j.ceramint.2018.07.216
Reference: CERI18938

To appear in: *Ceramics International*

Received date: 12 May 2018
Revised date: 20 July 2018
Accepted date: 24 July 2018

Cite this article as: Marija Nedeljković, Bahman Ghiassi, Stefan Melzer, Chris Kooij, Sieger van der Laan and Guang Ye, $CO_2$ binding capacity of alkali-activated fly ash and slag pastes, *Ceramics International,* https://doi.org/10.1016/j.ceramint.2018.07.216

# $CO_2$ binding capacity of alkali-activated fly ash and slag pastes

Marija Nedeljković [1], Bahman Ghiassi[2], Stefan Melzer[3], Chris Kooij[3], Sieger van der Laan[3], Guang Ye[1]

[1]Microlab, Faculty of Civil Engineering and Geosciences, Delft University of Technology, Stevinweg 1, 2628 CN Delft, The Netherlands

[2]Centre for Structural Engineering Design and Informatics, Faculty of Engineering, University of Nottingham, Nottingham, United Kingdom

[3]Tata Steel, R&D, P.O. Box 10.000, 1970 CA IJmuiden, The Netherlands

e-mail: M.Nedeljkovic@tudelft.nl
Bahman.Ghiassi@nottingham.ac.uk
stefan.melzer@tatasteel.com
chris.kooij@tatasteel.com
sieger.van-der-laan@tatasteel.com
G.Ye@tudelft.nl

* Corresponding author. Tel: +31 (0)15 278 4554



**Abstract**

Quantification of the $CO_2$ binding capacity of reinforced concrete is of high importance for predicting the carbonation potential and service life of these structures. Such information is still not available for alkali activated materials that have received extensive attention as a sustainable substitute for ordinary Portland cement (OPC)-based concrete. To address this gap, this paper evaluates the $CO_2$ binding capacity of ground powders of alkali activated fly ash (FA) and ground granulated blast furnace slag (GBFS) pastes under accelerated carbonation conditions (1 % v/v $CO_2$, 60% RH, 20°C) for up to 180 days. The $CO_2$ binding capacity, the gel phase changes, and the carbonate phases are investigated with complementary TG-DTG-MS, FT-IR and QXRD techniques.

Five mixtures with different FA/GBFS ratio are considered. CEM I and CEM III/B pastes are also studied to provide a baseline for comparisons. The results showed that the

alkali-activated pastes have a lower $CO_2$ binding capacity in comparison to cement-based pastes. Furthermore, alkali-activated pastes have similar $CO_2$ binding capacity regardless of the FA/GBFS ratio. It was observed that the silicate functional groups corresponding to the reaction products in the pastes were progressively changing during the first 7 days, after which only carbonate groups changed. It was also found that the $CO_2$ bound in the alkali-activated pastes occurs to a substantial extent in amorphous form.

Graphical asbtract

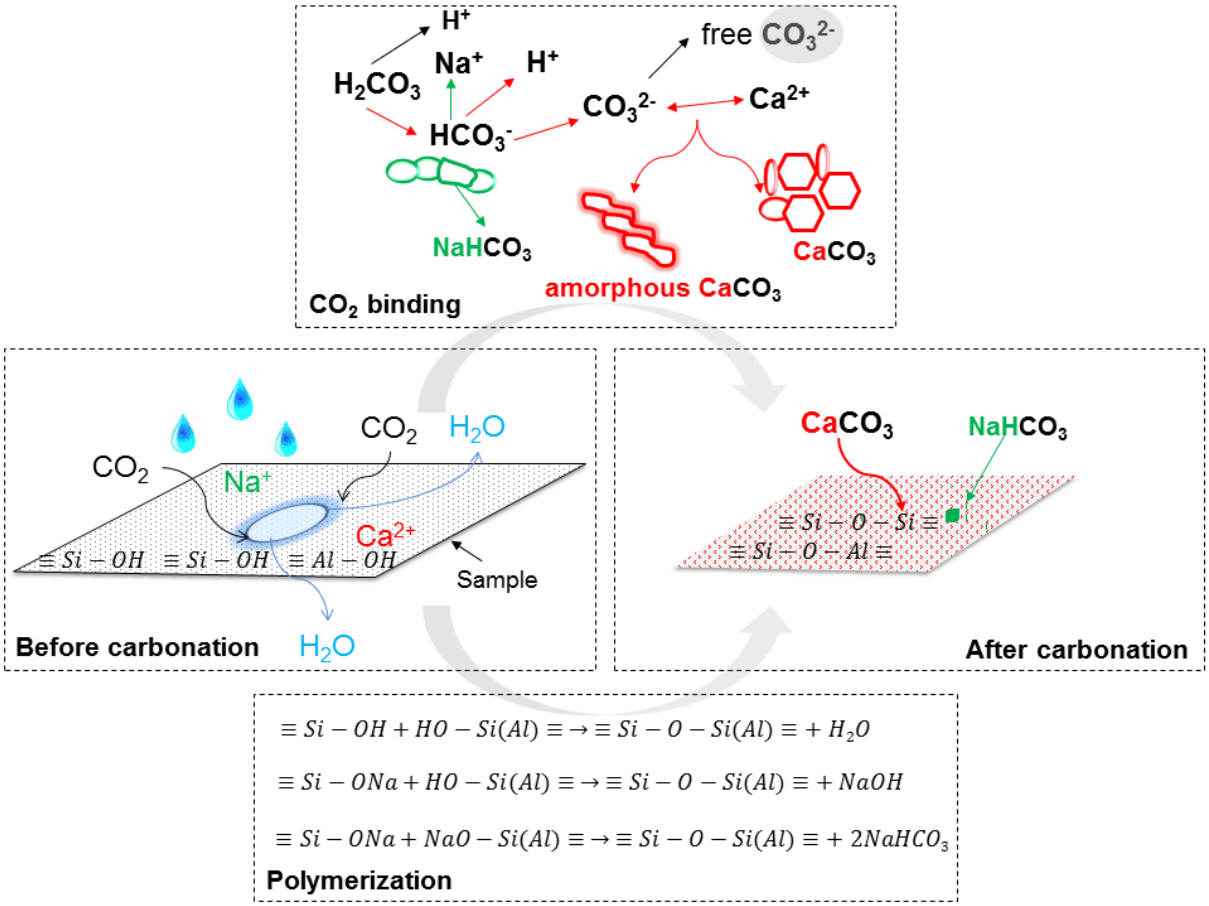


**Scheme 1.** Graphical abstract.

**Keywords:** Alkali-activated FA/GBFS; $CO_2$ binding capacity; TG-DTG-MS.

# 1. Introduction

Although recently there has been considerable attention for the possibility of using alkaline-activated materials (AAMs) in the construction sector, several issues regarding the long-term performance of these materials are still open [1, 2]. Carbonation of AAMs, as one of the main deterioration mechanisms in reinforced concrete, has been the subject of many studies [3-6]. But this complex deterioration process is still not well understood.

Carbonation is the result of reaction between carbonic acid (that forms in the pore solution due to dissolution of gasous $CO_2$) and $Ca^{2+}$ ions present in the pore solution [7]. The presence of portlandite ($Ca(OH)_2$) in Portland cement (OPC)-based concrete leads to saturation of the pore solution with $Ca^{2+}$ and $OH^-$ ions even after carbonation, thus buffering the pH level above 12. This intrinsically high pH of the pore solution results in formation of a thin passive layer around the steel bars protecting them against corrosion [8]. Consumption of $Ca^{2+}$ ions due to carbonation triggers dissolution of the portlandite (and calcium silicate hydrate (C-S-H)) to resaturate the pore solution. This cycle continues until the portlandite is fully consumed only after which the pH starts dropping. As C-S-H, monosulfate (AFm) and ettringite (Aft) phases are unstable at lower pH values, subsequently dissolution of these phases starts when the pH drops below 12.6 [7]. Further progress of carbonation leads to further reduction of the pH, and eventually to a certain level (around 9.5), where the protective layer on the steel bars is destroyed [8]. Additionally, carbonation often concurs with an increase of mechanical strength and refinement of the pore structure by precipitation of $CaCO_3$ in the pores of OPC-based materials [9]. In general, carbonation is controlled by both diffusion and chemical reaction. It is dependent on several factors including relative humidity, tortuosity of the paste, concenteration of $CO_2$ in the environment, and type and chemistry of the binder [10-12].

In AAMs the carbonation mechanisms are expected to be different from that of OPC-based concrete due to their fundamental differences in constituting phases and pore structure [13]. While the main reaction products in OPC-based materials are portlandite and C-S-H, different alkaline gel phases are formed in AAMs. These include sodium aluminosilicate hydrate (N-A-S-H), calcium aluminosilicate hydrate (C-A-S-H), calcium sodium aluminosilicate hydrate (C-N-A-S-H) [13-15]. AAMs do not contain portlandite [16] and have a lower reactive Ca-content in comparison to OPC-based materials. This leads to faster decalcification of C-A-S-H/C-N-A-S-H gels and may account for the faster carbonation process in AAMs [17, 18]. Furthermore, carbonation mechanism can be strongly influenced by the type of precursor (FA, GBFS, metakaoline) [5, 19], the nature and dosage of the alkaline activator used [3] as well as the exposure conditions [20], amongst others. An accurate quantification of the $CO_2$ binding capacity of AAMs is of critical importance for understanding the maximum carbonation degree and service life performance predictions.

To the authors' knowledge, however, there is still no such study aiming at quantification of the carbonation degree of AAMs. Carbonation in AAMs occurs in two main steps [21]: (1) carbonation of the pore solution leading to reduction of pH and precipitation of Na-rich carbonates; and (2) decalcification of Ca-rich phases and secondary products present in the system. This suggests that the $CO_2$ binding capacity of AAMs, in contrast to OPC-based materials, is not only a function of the reactive CaO content, but also influenced by the $Na_2O$ content consumed during the precursors (e.g. FA and GBFS) dissolution.

The main aim of this paper is to evaluate the $CO_2$ binding capacity, carbonation products and mineralogical changes of alkali-activated FA/GBFS pastes under accelerated carbonation conditions (1 % v/v $CO_2$, 60% RH, 20°C). The role of GBFS content in blended alkali-activated pastes on these parameters is investigated by considering five different mixtures with FA/GBFS ratio of 100:0, 30:70, 50:50, 70:30 and 0:100. CEM I and CEM III/B

pastes are also prepared and tested to provide a baseline for comparisons. The $CO_2$ binding capacity is evaluated with thermogravimetric (TG)-mass spectrometry (MS). The effect of accelerated carbonation on the gel molecular structure and minerology of AAMs is investigated with attenuated total reflectance Fourier Transformed Infrared spectroscopy (FT-IR) and quantitative X-ray diffraction (QXRD) analysis.

## 2. Materials and methods

### 2.1 Materials and sample preparation

FA and GBFS were supplied from VLIEGASUNIE BV and ORCEM, respectively, while CEM I 42.5 N and CEM III/B 42.5 N were supplied by ENCI (the Netherlands). The chemical composition of raw materials was determined with X-ray Fluorescence (XRF) (Table 1) with a Panalytical AXIOS Max Advanced XRF spectrometer. The analysis of raw materials was performed with fused beads and lithium tetraborate/methaborate as a flux. Sulphur (S) was determined with Eltra Sulphur analyzer. Loss on ignition (LOI) was determined with LECO Thermogravimetric Analyser (TGA701).

**Table 1** Chemical composition of FA, GBFS, CEM I and CEM III/B measured with XRF [%].

| | $SiO_2$ | $Al_2O_3$ | CaO | MgO | $Fe_2O_3$ | S | $Na_2O$ | $K_2O$ | $TiO_2$ | $P_2O_5$ | LOI |
|---|---|---|---|---|---|---|---|---|---|---|---|
| FA | 56.8 | 23.8 | 4.8 | 1.5 | 7.2 | 0.3 | 0.8 | 1.6 | 1.2 | 0.5 | 1.2 |
| GBFS | 35.5 | 13.5 | 39.8 | 8.0 | 0.6 | 1.0 | 0.4 | 0.5 | 1.0 | 0.0 | -1.3 |
| CEM I | 19.6 | 4.8 | 62.2 | 1.8 | 3.0 | 1.4 | 0.4 | 0.6 | 0.3 | 0.2 | 2.8 |
| III/B | 30.0 | 11.0 | 45.0 | 7.0 | 1.3 | 1.9 | 0.4 | 0.5 | 0.9 | 0.6 | 0.1 |

X-ray diffraction is used to study the minerology of raw materials (such as described in Section 2.2). Fig. 1 shows quantitative phase analysis results performed by Rietveld

method for GBFS, FA, CEM I and CEM III/B. The silicon standard was used to quantify the amount of amorphous phase of the samples. Fig. 1 shows that GBFS is fully amorphous, while FA is composed of amorphous and crystalline phases (such as quartz, mullite, magnetite and hematite). CEM I and CEM III/B have different mineral compositions. The CEM I consists of tricalcium silicate ($C_3S$), dicalcium silicate ($C_2S$), tricalcium aluminate ($C_3A$), tetracalcium aluminate ferrite ($C_4AF$) and small amounts of minor constituents like anhydrite ($CaSO_4$), calcite ($CaCO_3$), periclase, gypsum and quartz. XRD diffractogram of CEM III/B shows that it is predominantly amorphous.

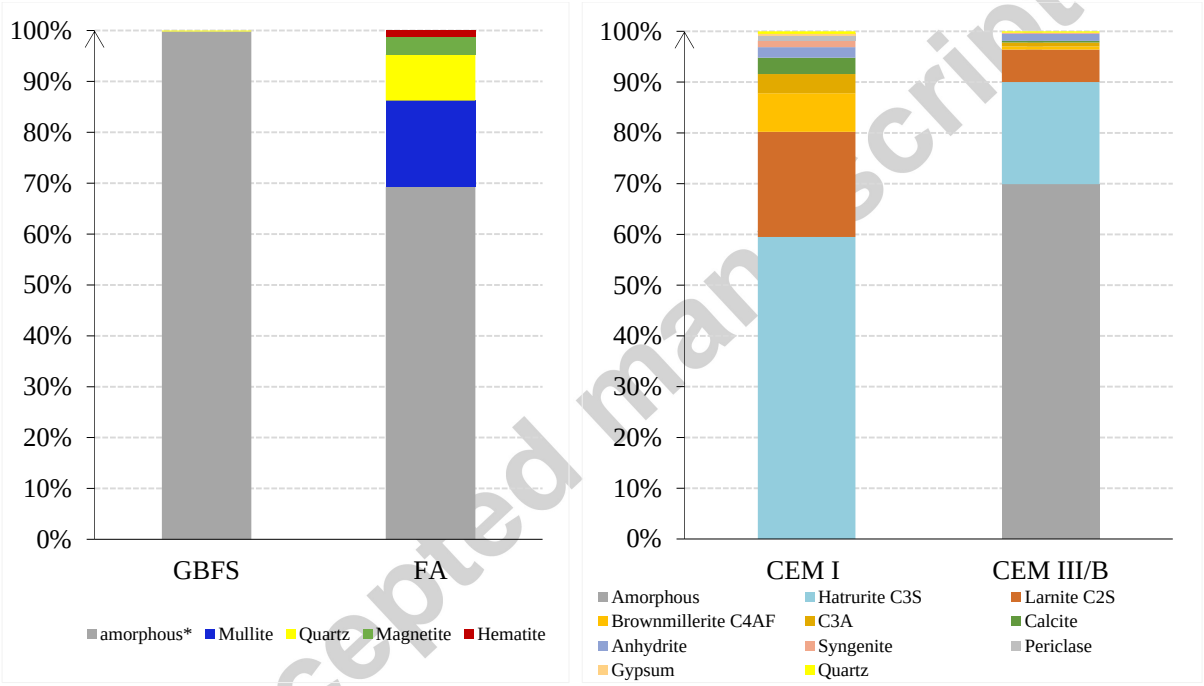


**Fig. 1.** Quantitative phase analysis by Rietveld method for raw materials: GBFS, FA, CEM I and CEM III/B.

The alkaline activator was prepared by mixing anhydrous pellets of sodium hydroxide with deionized water and sodium silicate solution (27.5 wt.% $SiO_2$, 8.25 wt.% $Na_2O$). After mixing, the activator was kept in laboratory conditions at a temperature around 20 °C to cool down for 24 h prior to the paste mixing. The activator $Na_2O$ concentration was 4.8 wt.% with

respect to the mass of precursors (FA + GBFS). For each paste, the activator liquid-to-binder mass ratio was 0.5. The pastes were produced with the following FA/GBFS ratios of 100:0, 70:30, 50:50, 30:70, 0:100 wt.%, named S0, S30, S50, S70, S100, respectively (Table 2). Cement pastes were made with water-to-binder ratio 0.5.

**Table 2** Mixture design for pastes with respect to 100 g of binder.

| Mixture | FA[a] | GBFS[b] | OPC[c] | $m(Na_2O)/m(binder)$ | $SiO_2/Na_2O$ | water/binder | liquid/binder |
|---|---|---|---|---|---|---|---|
| S0 | 100 | 0 | | | | | |
| S30 | 70 | 30 | | | | | |
| S50 | 50 | 50 | 0 | 4.80 | 1.45 | 0.38 | |
| S70 | 30 | 70 | | | | | 0.50 |
| S100 | 0 | 100 | | | | | |
| CEM III/B | 0 | 70 | 30 | - | - | 0.50 | |
| CEM I | 0 | 0 | 100 | | | | |

[a, b, c]weight percentage with respect to raw material (FA, GBFS, OPC) content (wt. %).

The precursors were dry-mixed for 2 minutes and then mixed with the activator. The pastes were cast in cylindric polyethylene jars, with 35 mm diameter and 70 mm height (Fig. 2) and vibrated for 15-30 s on a vibrating table. The samples were sealed cured until 28 days. The curing method was chosen based on previous study of authors which showed that unsealed wet curing of the samples result in substantial $Na^+$ loss [12].


**Fig. 2.** Bulk sample after demoulding (left), ground sample (middle), SEM-BSE image of the powder (right).

## 2.2 Test programme

Accelerated carbonation was performed on ground pastes in a carbonation chamber where $CO_2$ concentration, temperature and relative humidity were controlled simultaneously. The $CO_2$ concentration was kept constant at 1% by volume and the temperature and relative humidity were regulated at 20°C and 60%, respectively.

In order to examine the $CO_2$ binding capacity of the ground paste (Fig. 2), samples were prepared by grinding powders from the sides of the sealed cured paste cylinders using a diamond drilling tool. By dusting, the powder was evenly distributed over a paper for exposure in the carbonation chamber. The average particle size of the powder was 75 μm, still allowing full carbonation on a practical timescale [4]. The mechanism and degree of the carbonation were investigated through a complementary set of analytical methods, including TG-DTG-MS, FT-IR, XRD. The TG-DTG-MS allowed quantification of the $CO_2$ uptake. The FT-IR analysis was performed to investigate the alteration of the gel molecular structure after accelerated carbonation and to detect the carbonates as a basis for determining the presence of carbonation products. The XRD and quantitative XRD (QXRD) were used for identification of the carbonation products and their quantification in carbonated powders. It should be noted that the powders were analyzed with TG-DTG-MS, FT-IR, XRD, immediately after the exposure period without any pre-drying. Therefore, the results include also the moisture in the samples. However, small amounts of moisture do not affect quantification of the $CaCO_3$. The sample materials that were not exposed to carbonation are referred to “reference materials” or “0 h carbonation”, hereafter.

### 2.2.1 TG-DTG-MS

TG-DTG-MS method was used to quantify the uptake of $CO_2$ by the powders. The TG-DTG-MS tests were performed at 0 h, 28 days and 180 days. The measurements were performed on the samples shortly after collecting them from the carbonation chamber.

The thermobalance Netzsch STA 449 F3 Jupiter coupled with a mass spectrometer Netzsch QMS 403 C was used to accurately identify the $H_2O$ and $CO_2$ emissions for each temperature range. Samples of approximately 35 mg were placed in an alumina crucible and exposed under an inert atmosphere of argon to increasing temperatures ranging from 40°C to 1100°C at a heating rate of 10 °C/min. A blank curve, obtained under the same conditions with the same empty alumina crucible, was systematically subtracted. The Mass Spectrometer (MS) was coupled to the TG to allow separation of concurrent mass loss from $H_2O$ and $CO_2$ release. The response of a sample with unknown concentration of $CO_2$ was compared to the response of a standard sample with known concentration under identical analytical conditions. Calcite was defined as the standard for calibration of the mass loss upon heating. Calibration of the Mass Spectrometer response to the $CO_2$ release from this standard compound allowed quantification of the $CO_2$ release from more complex powders, that beside calcium carbonates contain other compounds as reaction products. The peak integral, i.e. the area under the MS $CO_2$ curve, was quantified using OriginPro 9 software for each paste.



### 2.2.2 FT-IR

The alteration of the gel molecular structure under accelerated carbonation was investigated with FT-IR. The silicate (Si-O-T, T=Si, Al) and carbonate groups ($CO_3^{2-}$) were characterized in powdered pastes at different time intervals: 0h, 0.5h, 1h, 3h, 6h, 12h, 24h, 48h, 7 days, 14 days, 28 days, 180 days. Around 35 mg of powder of each paste was collected

and subsequently measured with attenuated total reflectance Fourier transformed infrared (ATR-FT-IR). Spectra were acquired with PerkinElmer Spectrum 100, over the wavelength range of 4000 (2000) $cm^{-1}$ to 600 $cm^{-1}$ with a resolution of 4 $cm^{-1}$. A total of 16 scans were collected per measurement.

### 2.2.3 XRD

Powders for XRD measurements were collected from reference samples (no $CO_2$, 180 days of sealed curing) and at 180 days carbonations. A few grams (3-5 g) of each sample were additionally ground in a McCRONE micronizing mill to below 15 µm, with an internal standard of 10 wt. % metallic silicon added. Both sample and internal standard were premixed and ground for 20 minutes under cycloxhexan (~7 ml) using sintered corundum grinding elements. Afterwards, the slurry was poured into a ceramic dish and transferred to an oven. The slurry was kept for a few minutes at 65°C in the oven, and subsequently the dried powder was pressed in a bottom-loaded XRD holder and prepared for XRD measurement. XRD diffractograms were acquired from 10° to 130° 2-theta with a Bruker D4 diffractometer using Co-Kα radiation and a Lynxeye position-sensitive detector. The Bruker Topas software was used to perform Rietveld quantification of the phases. The Rietveld fitting error obtained on the amorphous phase in the samples, showed high-precision, with statistical errors generally less than 1.0 % absolute.

# 3. Results and discussion

## 3.1 Quantification of $CO_2$ binding capacity

Fig. 3a, b show the DTG curves along with identified temperature ranges of the dehydration and decarbonation of the phases in noncarbonated and carbonated cement and alkali-activated paste powders. Fig. 3a shows results for sealed cured, 180 days old pastes. In the reference CEM I and CEM III/B pastes, two peaks can be observed. The first peak at 50-200 °C temperature range is associated with the evaporation of free water and decomposition of hydrates. The second peak, at 450 °C, is assigned to dehydration of portlandite [22]. In contrast, in alkali-activated pastes, only one peak at temperature range of 50-200 °C is found, that is common for the dehydration of the gel phases (N-A-S-H, C-(N-)A-S-H) [5]. This clearly shows the absence of portlandite in alkali activated pastes.

The DTG curves of all the carbonated powders for 180 days of exposure showed a peak below 200 °C (Fig. 3b). Additionally, it can be observed that the portlandite is still remaining in the carbonated paste CEM I, whereas it has completely disappeared in the CEM III/B paste (Fig. 3). The broad peaks in the temperature range of 250-950 °C correspond to different metastable to stable carbonates. The relative intensities of these peaks changes with the GBFS content and becomes dominant with increasing the amount of GBFS.

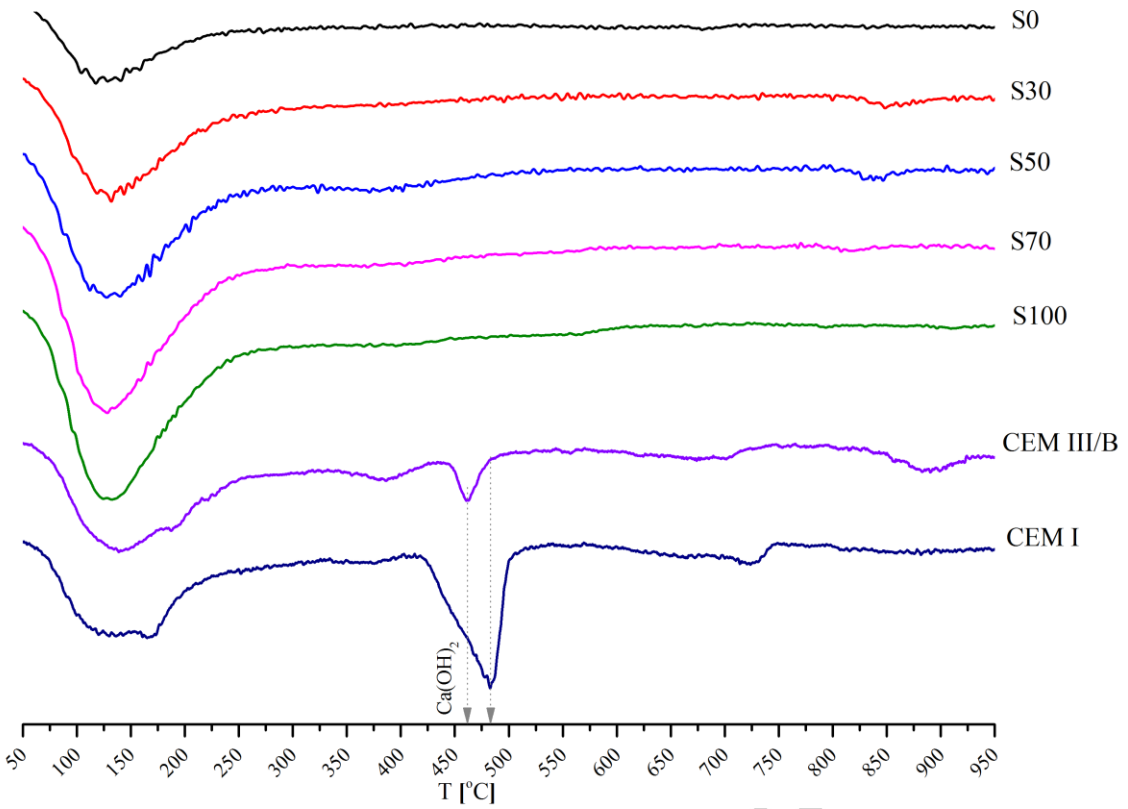


a) DTG curves for reference (noncarbonated) powders (after 180 days of sealed curing).

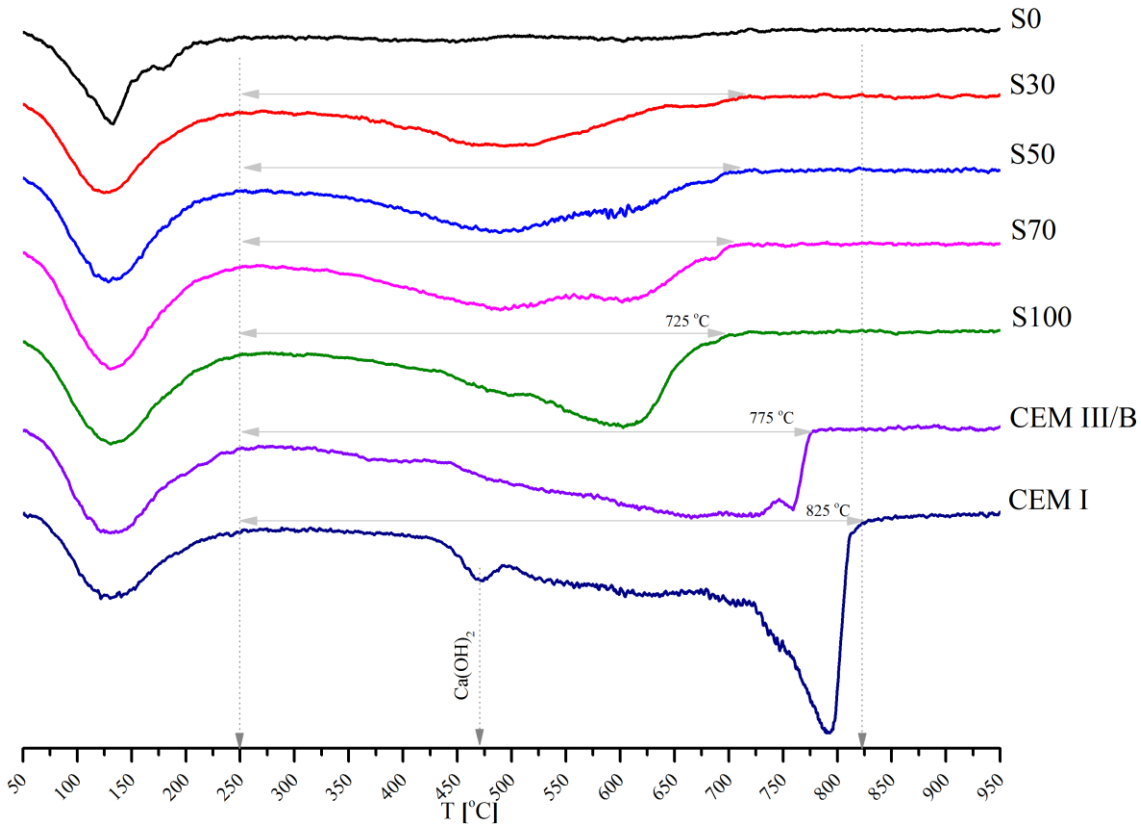


b) DTG curves for carbonated powders (after 180 days of carbonation).

**Fig. 3.** a. DTG curves for reference (noncarbonated) powders (after 180 days of sealed curing); b. DTG curves for carbonated powders (after 180 days of carbonation).

The MS $CO_2$ curves of the reference (0 h) and carbonated (28 days and 180 days) pastes are plotted in Fig. 4. The carbonate types present in the samples can be identified from the temperature ranges in which the $CO_2$ is released as follows:

- carbonates from the aqueous solution with lower temperature release between 100 ºC and 180 ºC, such as sodium bicarbonates/carbonates;
- amorphous carbonates with higher release temperatures between 245 ºC and 645 ºC;
- crystalline carbonates detected with XRD with known temperature release between 645 ºC and 745 ºC.

The quantity of each carbonate type can also be estimated from the area under the MS $CO_2$ curves in each of these temperature ranges. The TG-DTG-MS spectra show a minor release of $CO_2$ at around 100 ºC and the major release at temperatures above 300 ºC in all paste types. It also seems that a premature carbonation (at t=0 h) has taken place in most of the pastes. This is mainly due to the grinding of the pastes. Another interesting observation is that the $CO_2$ release ends at 650-700 ºC in alkali activated pastes that is lower than the maximum release temperature in cement-based pastes (750 ºC).

In alkali activated pastes (except S0), a small but distinct $CO_2$ release peak is observed at 675 ºC only in 180 days carbonated samples. In the temperature range of 300 ºC to 650 ºC, all the pastes show multiple release peaks after exposure to accelerated carbonation. These peaks are clearly observable at 500 ºC and at 600 ºC in alkali activated pastes. In blended pastes (i.e. S30, S50 and S70), there is a significant difference between the peaks at 500 ºC in 28 days and 180 days carbonated samples, but the peaks at at 600 ºC do not show significant differences. Interestingly, this peak (at 600 ºC) is almost absent in the paste S30. Additionally,

paste S0 shows a distinct $CO_2$ emission at 140 °C that can be attributed to the nahcolite decarbonation as also observed in XRD analyses (Fig. 8) and previously reported data in the literature [5]. These results show that depending on the type of pastes various forms of carbonates are formed under accelerated carbonation tests.

In general, the total $CO_2$ release has increased from 28 days to 180 days in alkali activated blended pastes showing that carbonation has been progressing during this period. This is similar to CEM I and CEM III/B pastes in which the released $CO_2$ between 28 days and 180 days was significantly increased in the temperature range of 550 °C to 800 °C. On the contrary, S0 paste hardly binds any $CO_2$ and S100 paste shows little difference between the $CO_2$ release of 28 and 180 days of carbonation.

It is known that $CaCO_3$ can precipitate from aqueous solution in various metastable forms [23, 24], while $CO_2$ is likely to be present as adsorbed $CO_2$ or carbonate/bicarbonate ions in solution (such as $CO_3^{2-}$ or $HCO_3^-$) [25]. The simultaneous presence of amorphous $CaCO_3$, metastable $CaCO_3$ (vaterite and aragonite) and calcite in the carbonated powder makes it difficult to carry out a rigorous separation of temperature ranges for their decomposition. However, this does not affect calculations made for determination of the total bound $CO_2$.

The bound $CO_2$ calculations show that, on average, 10-36 % $CO_2$ by mass of pastes was bound after 180 days through formation of Ca- and/or Na- carbonates (Table 4). It can be observed that the identified $CaCO_3$ is mainly crystalline in S100 paste, while, it is mainly amorphous in all other alkali-activated pastes. It also seems that the alkali-activated pastes take up similar amounts of $CO_2$ after 180 days of exposure.

Pastes S70 and S100, although having a higher CaO content in their chemical composition (Table 1), have a lower bound $CO_2$ compared to other pastes. This may seem contradictory to the XRD results (Fig. 9), but it should be noted that the total amount of

crystalline $CaCO_3$, determined with QXRD, underestimates the $CO_2$ amount quantified by thermal analysis [26]. This can be the reason for the observed difference between the TG-DTG-MS and QXRD results as various forms of $CO_2$ appeared in the samples, including adsorbed $CO_2$ in the C-(N-)A-S-H gel and pore solutions, amorphous $CaCO_3$ (that all can not be detected with XRD), as well as chemically bound $CO_2$ in crystalline phases $NaHCO_3$ and $CaCO_3$ polymorphs. The variation of temperatures at which these carbonates are released from the pastes, stems from the differences in the gel's chemical and molecular structure in these pastes. The carbonation of gel phases with different Ca/Si ratio, i.e. with different intrinsic atomic ordering of calcium (alumino) silicate hydrates, will certainly lead to structurally different types of carbonates, as will be shown in Section 3.3.

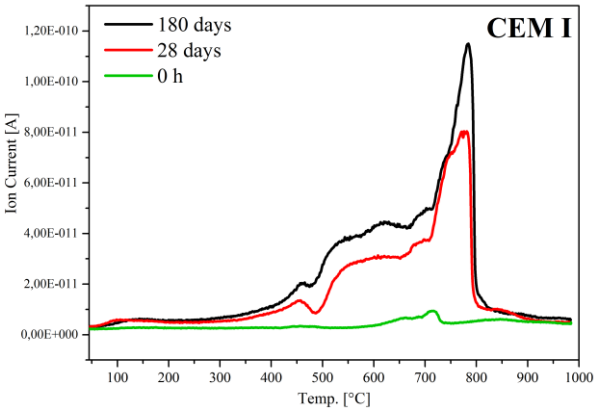


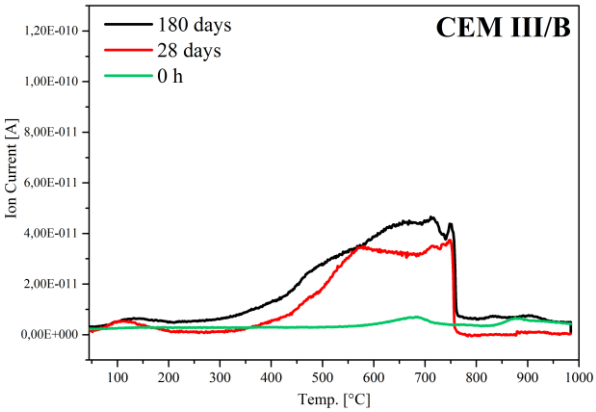


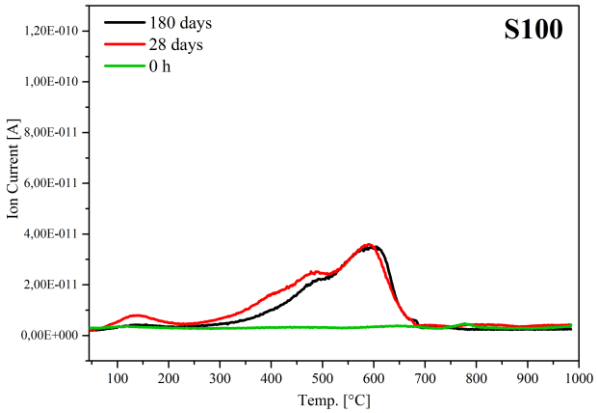


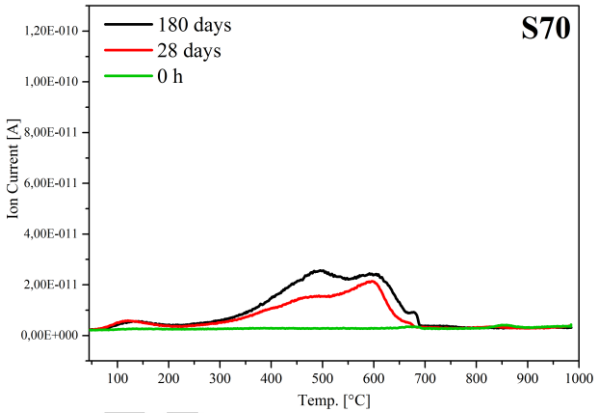


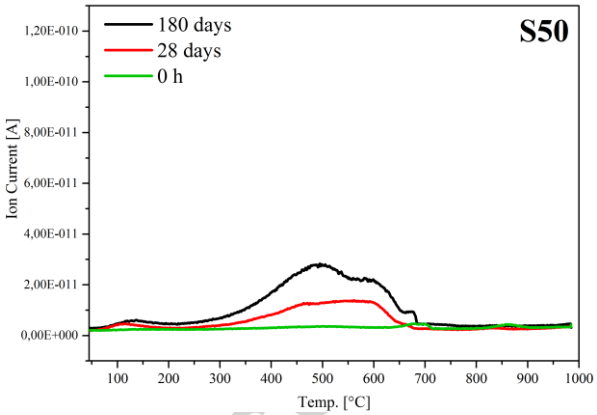


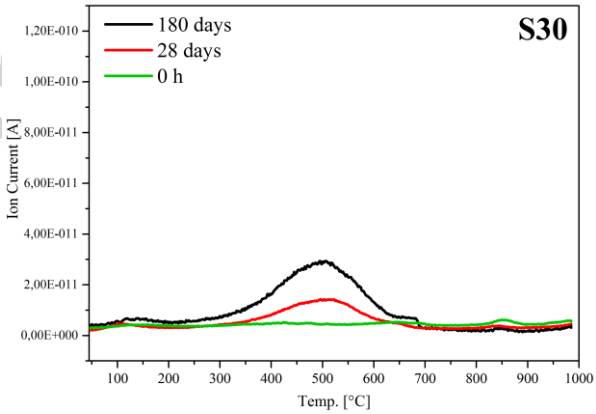


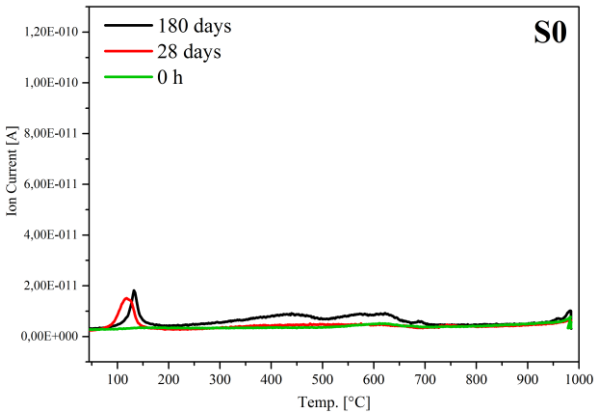

**Fig. 4**. MS $CO_2$ curves of reference paste powders (samples before carbonation, 0 h, green lines), MS $CO_2$ curves of paste powders obtained after 28 days of continuous carbonation (red lines), MS $CO_2$ curves of paste powders obtained after 180 days of continuous carbonation (black lines), (exposure conditions: $CO_2$ 1% v/v, 20°C, 60 %RH).

### 3.2 Molecular analysis of the functional groups

The FT-IR technique was used to monitor the changes of the functional groups of the reaction products during carbonation. This information is critical for comprehensive understanding of the gel carbonation at molecular level. Three major functional groups are distinguished:

- water region ($H_2O$ and OH),
- Si–O–Si (Al) region,
- carbonate region (O-C-O).

The FT-IR spectra and the characteristic frequencies of pure Ca-carbonates obtained from [27, 38] and Na-carbonates are used to differentiate formation of different carbonate phases in carbonated pastes of this study (Table 3). All the samples were cured for 28 days under sealed conditions before they were carbonated. The FT-IR spectra of reference and carbonated pastes are compared in Fig. 5. Separate presentation of the reference spectra (after 180 days of sealed curing) and spectra of pastes at 28 days and 180 days of carbonation is made in Fig. 6 for clarity of analysis.

Table 3 Characteristic frequencies in Na- and Ca-carbonates [$cm^{-1}$]. The FT-IR data for Na-carbonates were obtained from pure compounds. The FT-IR data for Ca-carbonates were obtained from [27, 38].

| | $\nu_3$ | $\nu_1$ | $\nu_2$ | $\nu_4$ |
|---|---|---|---|---|
| Nahcolite ($NaHCO_3$) | 1450 | 1032, 1046 | 831 | 686 |
| Natrite ($Na_2CO_3$) | 1381 | | 885 | 700 |
| Amorphous ($CaCO_3$) | 1475, 1420 | 1070 | 875 | 715 |
| Vaterite ($CaCO_3$) | 1490, 1420 | 1085, 1070 | 875, 850, 830 | 750 |
| Aragonite ($CaCO_3$) | 1489, 1475 | 1080 | 856 | 713, 700 |
| Calcite ($CaCO_3$) | 1430, 1419.6 | | 875, 845 | 715 |

**Water region ($H_2O$ and OH)**

The presence of $H_2O$ is detected by two characteristic absorption bands in the 3700-2500 $cm^{-1}$ region (corresponding to the stretching and deformation modes of $OH^-$) and in the 1640 $cm^{-1}$ region (associated with bending vibration mode of $H_2O$) that is in agreement with the literature [28]. The important difference between the reference cement-based and alkali-activated paste powders (0 h, Fig. 5) is situated in the region of the $OH^-$ group (3700-2500 $cm^{-1}$ region). In the cement paste powders (CEM I and CEM III/B) this band is at 3642 $cm^{-1}$. This band is assigned to $OH^-$ group of portlandite, which is absent in the FT-IR spectra of

alkali-activated pastes. This shows the absence of portlandite as also shown by the TG-DTG-MS spectra (Fig. 3a).

The intensity of the $OH^-$ group band related to portlandite, at 3642 $cm^{-1}$, in pastes CEM I and CEM III/B gradually decreased (0-28 days of carbonation, Fig. 5) until it completely disappeared at 180 days of accelerated carbonation (Fig. 6). Carbonation, in general, lead to reduction of water-related bands, at 3700-2500 $cm^{-1}$ and 1640 $cm^{-1}$, in all the pastes (Fig. 6). This is in agreement with the reduced release of water in DTG curves (Fig. 3a and Fig. 3b). This reduction is the most significant for the alkali-activated pastes.

**Si–O–Si (Al) region**

Position of silicate groups (symmetric stretching bands ~950 $cm^{-1}$, Si-O-T (with T = Si, Al**))** in FT-IR spectra indicates the difference of gel molecular structure in the alkali-activated pastes and cement pastes (most deviant for S0 and cement-based pastes, the latter with a double peak at 1120 $cm^{-1}$ and ~950 $cm^{-1}$, Fig. 5). Depending on the connectivity of silicon sites in silicate glasses as visualized in Scheme 2, the $SiQ^4$ unit has an IR absorption band centered around 1200 $cm^{-1}$, the $SiQ^3$ unit around 1100 $cm^{-1}$, the $SiQ^2$ unit around 950 $cm^{-1}$, the $SiQ^1$ unit around 900 $cm^{-1}$ and the $SiQ^0$ unit around 850 $cm^{-1}$ [29].

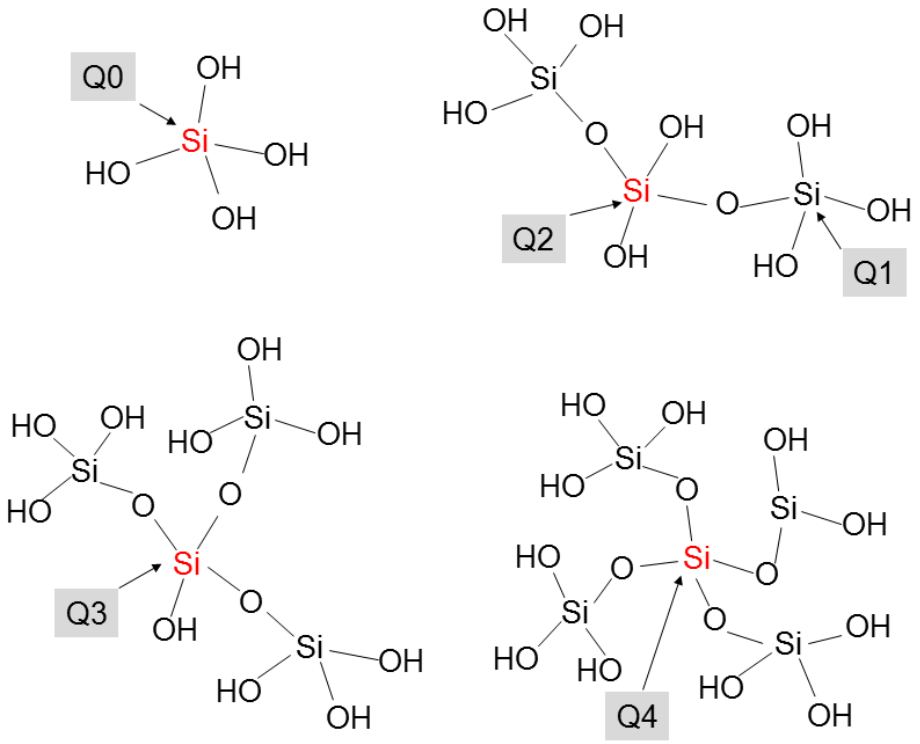


**Scheme 2.** Connectivity of silicon sites in silicate glasses.

Regardless of the type of the paste, the IR absorption band implies that the $SiQ^2$ was the main unit in the gel structure of the studied pastes before carbonation. The Si-O-T (T = Si, Al) stretching band appears at approximately 1015 $cm^{-1}$ for the carbonated powders containing GBFS, while the same band in the reference powders appears around 950 $cm^{-1}$ (Fig. 5). This shift is caused by gradual polymerization of the orthosilicate units ($SiO_4^{4-}$) in the reaction products of cement and GBFS pastes, i.e. the C-S-H, C-(N-)A-S-H gels, yielding $Q^2$ and $Q^3$ silicate units (Fig. 5). Meanwhile, as the FA-rich pastes are predominantly amorphous aluminosilicate materials, they likely consist of both Si-OH and Al-OH groups and therefore can be subjected to polymerization of Si-O-Al [30]. Namely, the extraction of the network modifyers (Ca, Na) from the gel interlayers as a result of carbonation leads to an excess of negative charge which is subsequently eliminated by adsorption of the cations (mostly $Na^+$) from the pore water. A similar process also occurs in carbonated OPC-based pastes as reported by Anstice et al. [31].

The carbonation process is described with chemical reactions 1-3, where *a*, b, c, d, e, and f are the stoichiometric coefficients for the respective oxide components CaO, $Na_2O$, $Al_2O_3$, $SiO_2$ and $H_2O$. The coefficients are different for each of the studied mixtures.

$$CO_2(aq) + H_2O \rightarrow H_2CO_3 \rightarrow HCO_3^- + H^+ \rightarrow CO_3^{2-} + H^+ \quad (1)$$

$$H_2CO_3 + 2NaOH \rightarrow Na_2CO_3 + 2H_2O \quad (2)$$

$$aNa_2CO_3 + (CaO)a(Na_2O)b(Al_2O_3)c(SiO_2)d(H_2O)e \rightarrow$$
$$aCaCO_3 + (Na_2O)b(Al_2O_3)c(SiO_2)d(H_2O)f + 2aNaOH + (e-f)H_2O \quad (3)$$

When no cations are available to preserve the charge equilibrium, neighbouring groups Si-OH, Si-ONa, Al-OH or Al-ONa condense and merge to Si-O-Si or Si-O-Al gel. The reactions taking place during the process are considered in 4-6.

$$\equiv Si - OH + HO - Si(Al) \equiv \ \rightarrow \ \equiv Si - O - Si(Al) \equiv + H_2O \quad (4)$$

$$\equiv Si - ONa + HO - Si(Al) \equiv \ \rightarrow \ \equiv Si - O - Si(Al) \equiv + NaOH \quad (5)$$

$$\equiv Si - ONa + NaO - Si(Al) \equiv \ \rightarrow \ \equiv Si - O - Si(Al) \equiv + 2NaHCO_3 \quad (6)$$

The intensities of silicate functional groups in pastes did not undergo further changes after 7 days of accelerated carbonation (Fig. 5). It appears that most of the pastes have been largely polymerized after 7 days of exposure in the carbonation chamber based on the FT-IR time-series measurements (Fig. 5). Both silicate and carbonate changes are the least apparent

for the paste S0. This suggests that the gel in this paste did not carbonate as earlier demonstrated by the TG-DTG-MS spectra. The $CO_2$ was mainly present as adsorbed on the N-A-S-H gel or in aqueous solution. This, also, is consistent with study of Bernal et al. [5].

The silicate band in paste CEM I (950 $cm^{-1}$→1075 $cm^{-1}$) shifts more compared to silicate band in paste CEM III/B (960 $cm^{-1}$→1021 $cm^{-1}$) and alkali-activated pastes after carbonation (950 $cm^{-1}$→1015 $cm^{-1}$). The magnitude of this shift is indicative of the polymerization degree [32], which is in this study lower for alkali-activated pastes (65 $cm^{-1}$) and paste CEM III/B (75 $cm^{-1}$), compared to carbonated paste CEM I (125 $cm^{-1}$). Comparing the magnitude of Si-T shift from this study with that of reported by Li et al. [3] and of Palacios et al. [17], it can be deduced that carbonated alkali-activated slag can polymerize even further after carbonation (1031 $cm^{-1}$) than observed in this study (1015 $cm^{-1}$). Concerning the $CO_2$ concentration used in this study (1% v/v) and from [3] (20% v/v) and [17] (100% v/v) it can be concluded that the degree of gel polymerization increases with the $CO_2$ concentration, in agreement with the findings of Castellote et al. [33].

**Carbonate region (O-C-O)**

The FT-IR spectra of carbonated pastes show the third type of bands, i.e. the carbonate bands. Three types of carbonate bands can be observed: strong broad band at 1408-1470 $cm^{-1}$ due to the asymmetric stretching of $CO_3^{2-}$ ($v_3$), narrow band at 875-856 $cm^{-1}$ representing the bending ($v_2$) of $CO_3^{2-}$, and the band at 713 $cm^{-1}$ in-plane bending ($v_4$) of $CO_3^{2-}$. Most of these bands correspond to amorphous $CaCO_3$, vaterite, aragonite and calcite characteristic bands as it can be deduced by comparison to the frequencies of their pure chemical compounds (Table 3) provided from [27].

After first 0.5h of the $CO_2$ exposure, the $CO_2$ uptake was recorded through appearance of carbonate bands at 1400-1500 $cm^{-1}$. This implies that the carbonation rate for powdered paste samples is initially controlled by the sorption of $CO_2$ at surface sites rather than by the rate of chemical reaction at the surface consistent with the study of Reardon et al. [34] for carbonation of cement powder paste under high $CO_2$ pressure. Additionally, $CO_2$ uptake is more pronounced in cement-based pastes than in alkali-activated pastes. This can be seen through the increase of the intensity of the bands at 1400-1500 $cm^{-1}$ region after 0.5 h. This is mainly due to higher CaO content in the cement-based pastes and hence higher affinity of cement-based pastes to adsorb $CO_2$. Hence the influence of composition of starting gel phases in the pastes on the $CO_2$ uptake is considerable. The evolution of $CO_2$ uptake with the progress of carbonation from 7 days to 28 days was slower than in the first 7 days with an initial rapid $CO_2$ uptake. Although FT-IR spectra show an intermediate $CO_2$ uptake occurring between 7 and 28 days, the $CO_2$ uptake varied between pastes in period of 28 days to 180 days (Fig. 6). It can be seen that in pastes S50, S70 and S100 in carbonate region (1400-1500 $cm^{-1}$) the right shoulder around 1400 $cm^{-1}$ disappears with elapse of carbonation time and that left shoulder close to 1500 $cm^{-1}$ became larger after 7 days of exposure, even more pronounced in the GBFS-rich pastes. It is assumed that in the first several hours of carbonation $CO_2$ is combined with gel phases, whereas in later ages, between 48 hours and 28 days, $CO_2$ is gradually released and forms aragonite (pastes S50, S70, S100) according to Table 3 and QXRD results in Fig. 8. The formation of aragonite was concurrent with the presence of amorphous silica in the samples as also observed by previous study [35].

Rafai et al. [36] reported similar behavior of $CO_2$ transformation during early carbonation of cement-based concrete. Using stable isotope $^{18}O$ and $^{13}C$, authors found that the initial $CaCO_3$ has a distinct isotope composition and a large quantity of $CO_2$ was combined with C-S-H gel. The $CO_2$ was then gradually released and produced another

$CaCO_3$, which was characterized by a much larger $^{18}O$ content than the initial $CaCO_3$. Similarly, Black et al. [35] reported the amorphous calcium carbonate as the first carbonation product from studies of the C-S-H carbonation at a longer time scale, formed presumably by the physical adsorption of $CO_2$ on the C-S-H gel surface. The subsequent formation of crystalline $CaCO_3$ polymorphs depended upon the Ca concentration and Ca availability in the surface layers as seen in this study. Different crystalline forms of the same compound ($CaCO_3$) exhibit slightly different IR spectra (spectra between vaterite, aragonite, calcite), the so-called polymorphism effect [37]. This is reflected in the FT-IR spectra for most of the studied pastes.

While paste S0 shows hardly any carbonate bands, the intensity of the broad 1400-1500 $cm^{-1}$ bands increased with GBFS content (from paste S30 to paste S100). Pastes S30, S50, S70 and S100 contain a sharp carbonate peak at 856 $cm^{-1}$ and only S30 has a second sharp peak at 875 $cm^{-1}$. Additionally, the broad, unsplit band in the range 1400-1500 $cm^{-1}$ represents amorphous $CaCO_3$ [38] and it is characteristic of the sample S30. This observation is in agreement with the decomposition of amorphous phase of the sample S30 demonstrated by the mass spectrometry analysis (Fig. 4). In contrast, FT-IR spectra of the carbonated samples S50, S70 and S100 (Fig. 5) contain well-resolved $v_3$ doublets with maximum at 1470 $cm^{-1}$, corresponding to aragonite [38], as confirmed with XRD analysis (Fig. 9). The cement-based pastes contain also three $CaCO_3$ polymorphs, vaterite, aragonite and calcite.

The calcite band in cement-based pastes at 875 $cm^{-1}$, overlaps with vaterite band according to the frequency ranges for vaterite and calcite carbonate groups in Table 3. To further examine the presence of different $CaCO_3$ and their proportions, and also of Na-carbonates (since the appearance of Na-carbonates in FT-IR spectra is not clear), XRD analysis is followed in the next section.

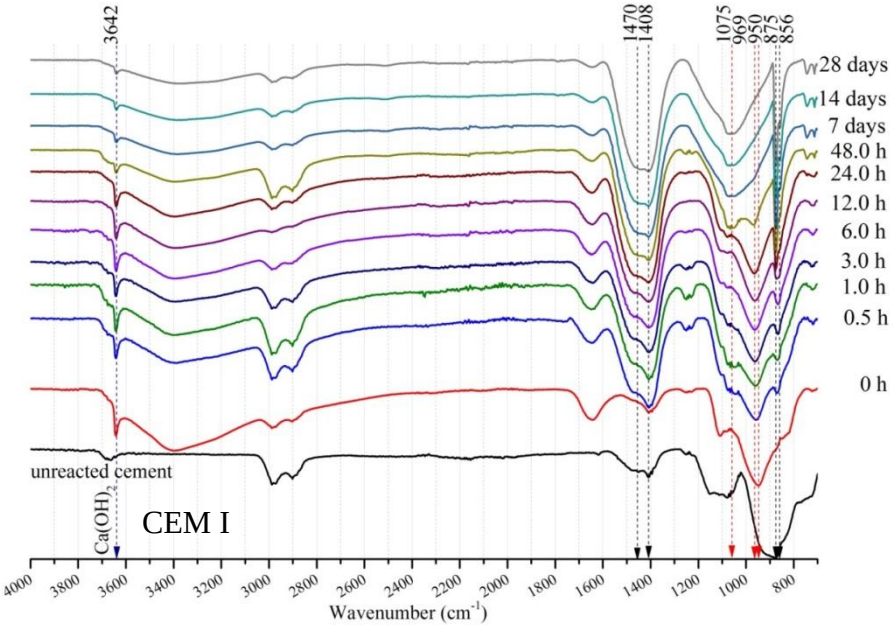


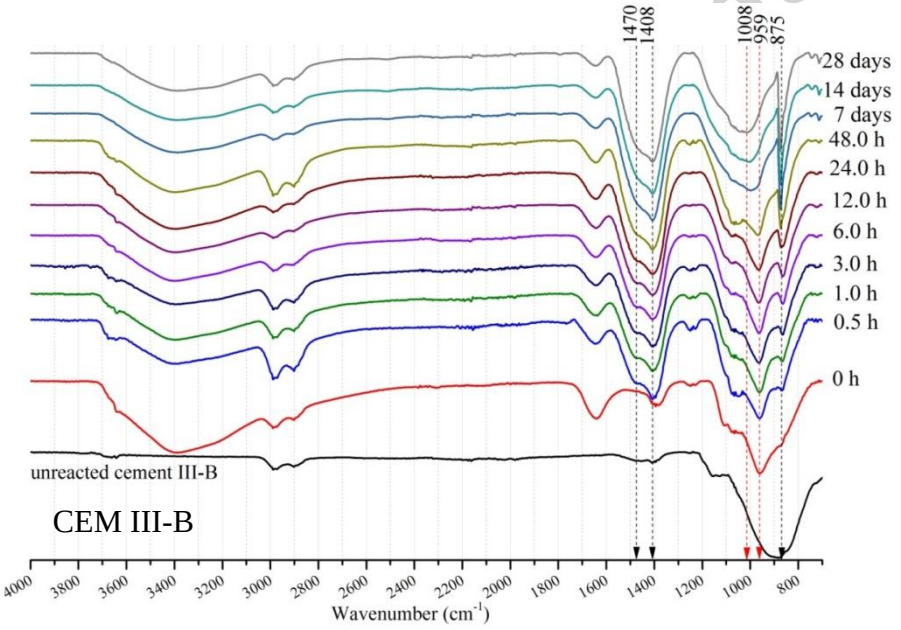

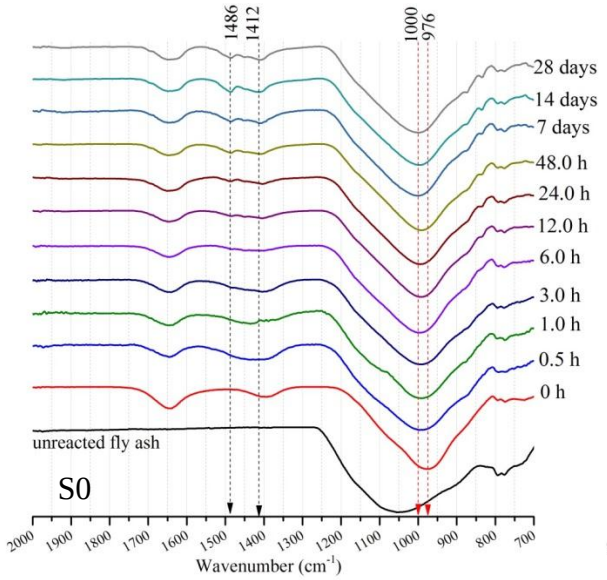


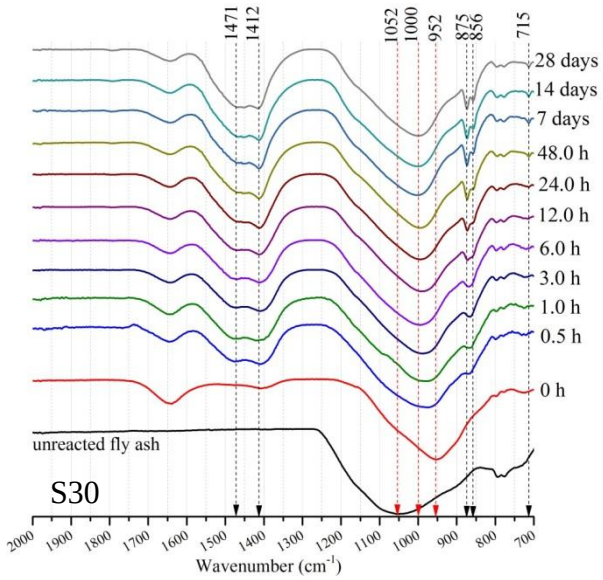


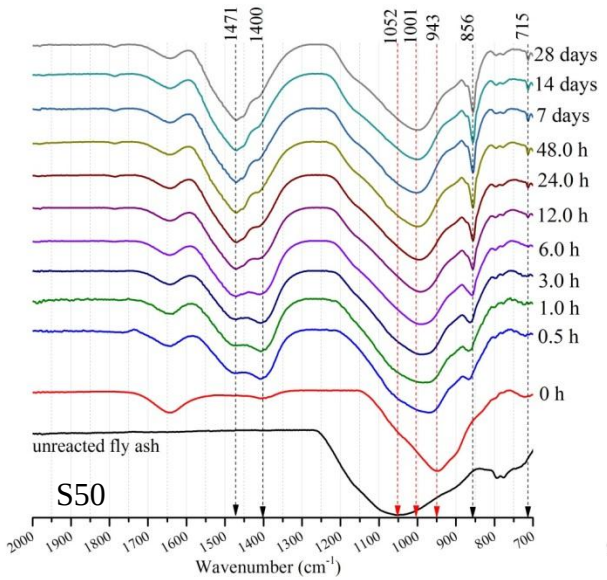


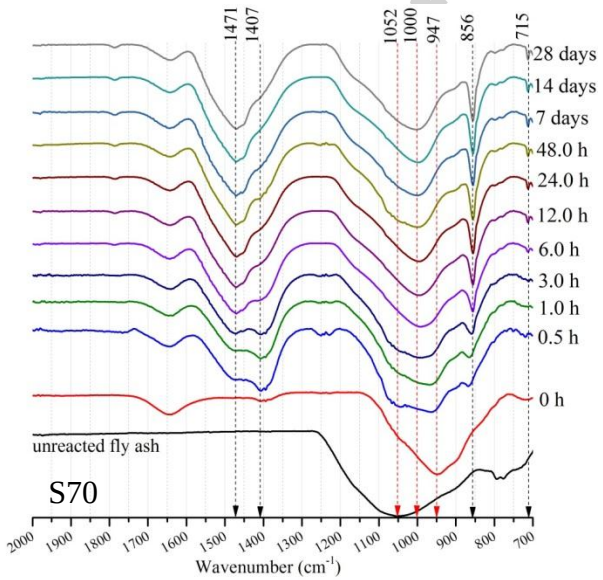


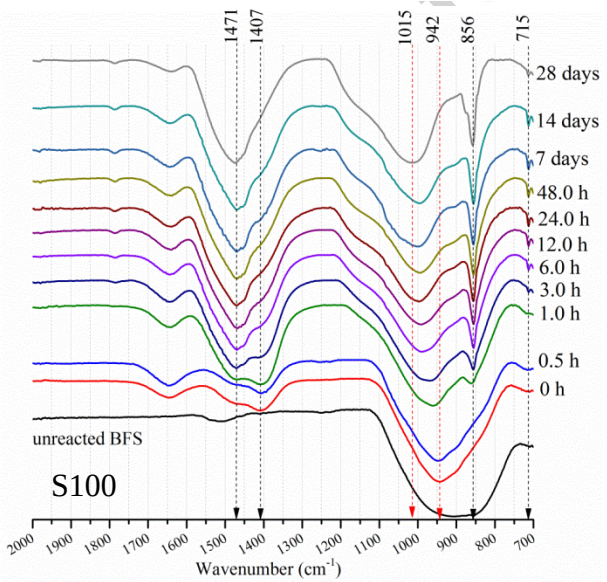

**Fig. 5.** FT-IR spectra of cement pastes (CEM I and CEM III/B) alkali-activated FA/GBFS pastes from time zero of exposure until 28 days (exposure conditions: 1% $CO_2$, 60 %RH)

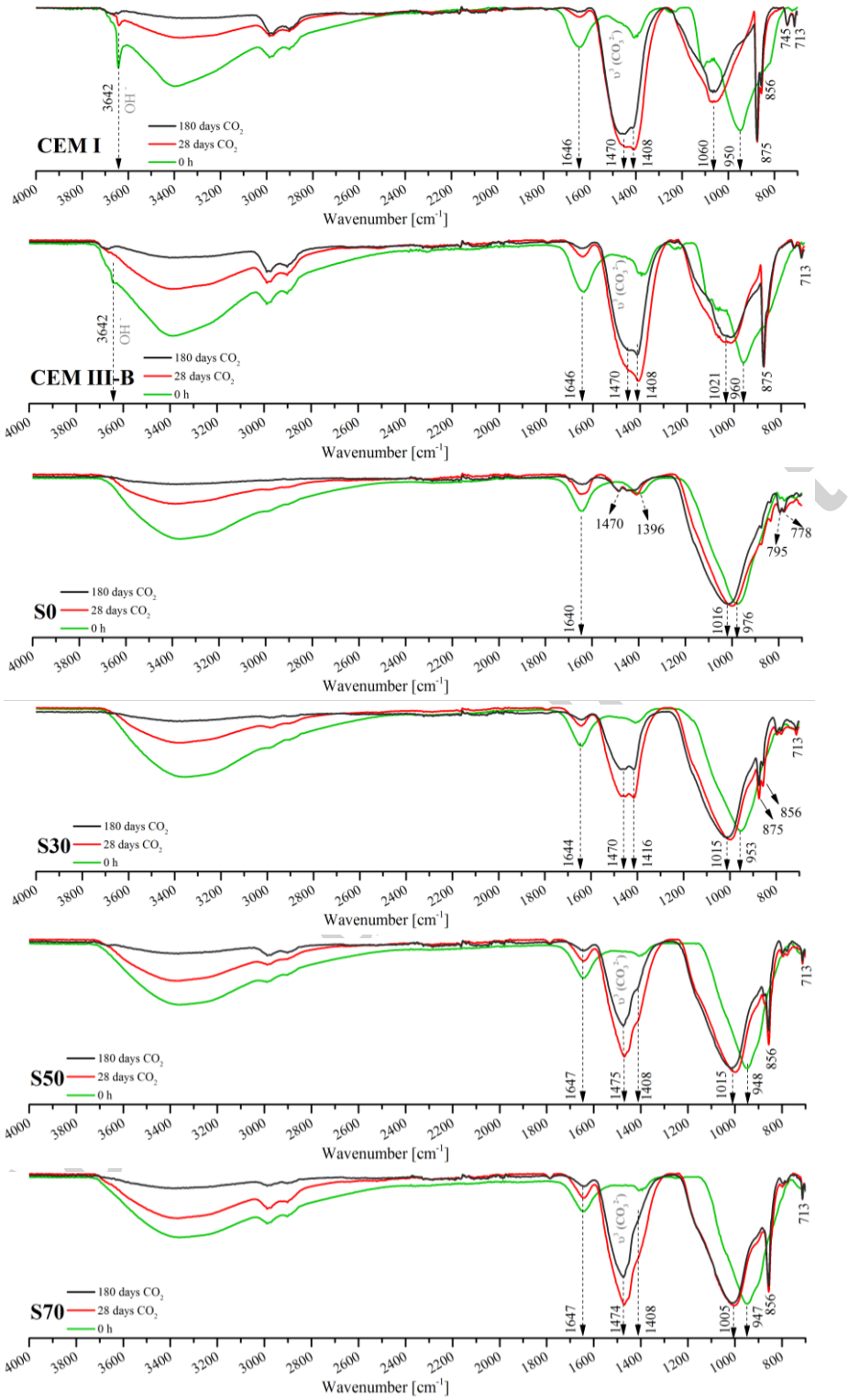

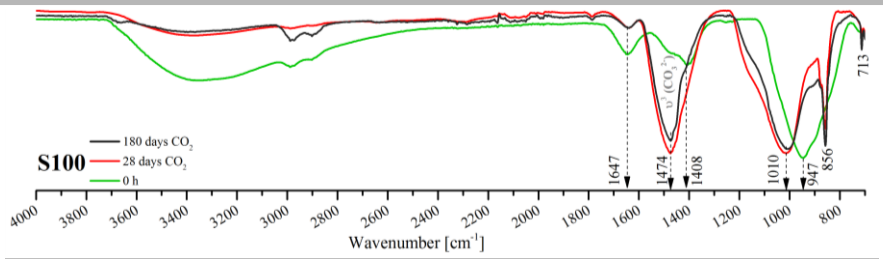


**Fig. 6.** FT-IR spectra of reference paste powders (samples before carbonation, 0 h, green lines), MS $CO_2$ curves of paste powders obtained after 28 days of continuous carbonation (red lines), MS $CO_2$ curves of paste powders obtained after 180 days of continuous carbonation (black lines), (exposure conditions: $CO_2$ 1% v/v, 20°C, 60 %RH).

### 3.3 Crystalline carbonate phases

To confirm the transformation of gel phases to various types of metastable (vaterite, aragonite) and stable $CaCO_3$, phase identification and quantitative analysis with XRD/QXRD was performed to complement the FT-IR identifications in Section 3.2. Fig. 7 shows XRD diffractograms of CEM I and CEM III/B pastes along with identified and quantified carbonation products (Table 4) for carbonated cement-based paste powders after 180 days of carbonation. It can be seen that the amorphous phase is dominant and its content is significantly higher in CEM III/B than in CEM I paste. The presence of remaining portlandite in the carbonated powder of the paste CEM I and its absence in paste CEM III/B is clear. This residual portlandite in the paste CEM I was also found in TG-DTG analyses. Hydrotalcite was found in paste CEM III/B, resulting from the high MgO content in this paste compared to paste CEM I, where MgO is very low (Table 1). Regarding the carbonation products, vaterite, aragonite and calcite were found in both pastes CEM I and CEM III/B.

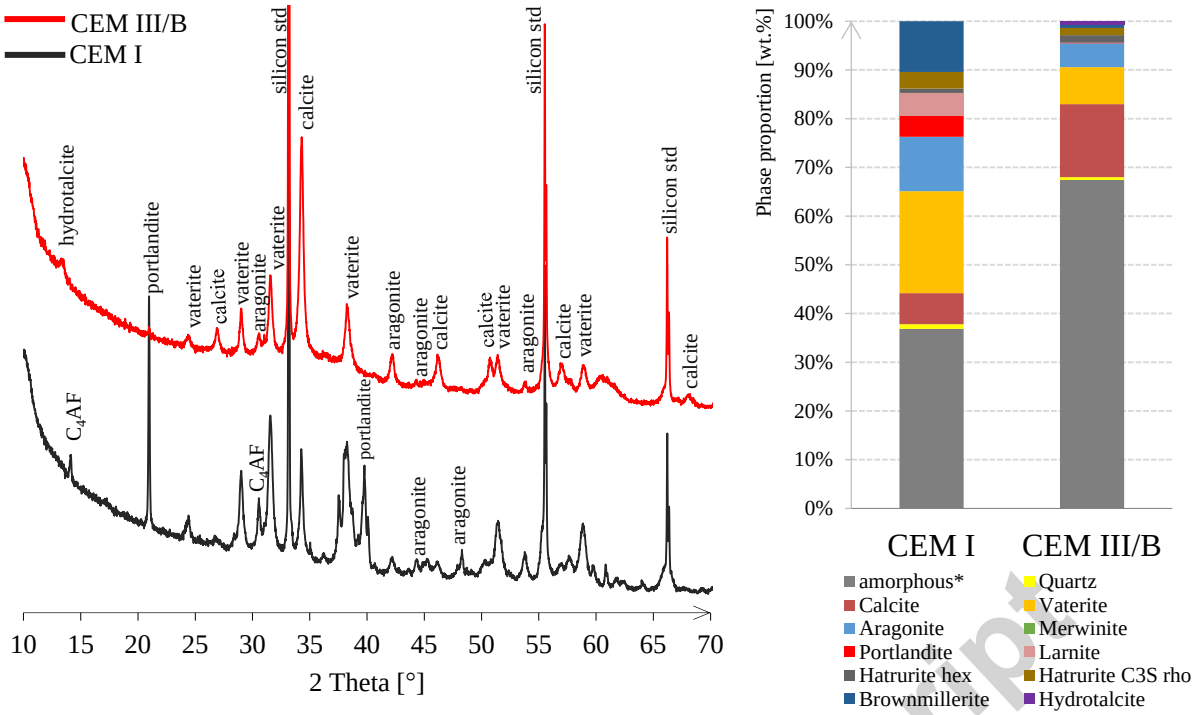


**Fig. 7.** XRD diffractograms with respect to the phases in: CEM I and CEM III/B carbonated powders (left), quantitative phase analysis by Rietveld method for cement paste carbonated powders after 180 days carbonation (right).

Fig. 8 shows the recorded XRD diffractograms along with identified carbonation products for reference alkali-activated pastes (noncarbonated powders) and for carbonated powders after 180 days of carbonation. Similar to paste CEM III/B, in alkali-activated pastes (S0→S100), the amorphous phase is dominant (Fig. 9). The pastes containing FA showed peaks for quartz, mullite, hematite and magnetite. Comparison of the XRD diffractograms of noncarbonated and carbonated pastes shows several additional peaks formed in the carbonated samples (Fig. 8). These peaks showed that nahcolite is a carbonation product in paste S0 as also found by Bernal et al. [5]. Aragonite was a dominant carbonation product in S50, S70 and S100, but this was not the case for paste S30 as also observed in FT-IR spectra (Fig. 5). The amount of calcite was found to be higher than aragonite in paste S30.

It is known that the resulting $CaCO_3$ polymorph depends on the conditions of carbonation such as relative humidity, temperature, $CO_2$ concentration as well as type of cement [9], but also on the experimental conditions during preparation of the powder. It should be noted that these factors can also affect the quantitative phase analysis by Rietveld method and can be a reason for such a high amount of calcite observed in the paste S30 compared to the other pastes. In Fig. 4 (MS $CO_2$), paste S30 has decarbonation at temperatures in the range of amorphous calcium carbonates, which cannot be identified with XRD. In addition, the small peak around 675°C appears in paste S30 (Fig. 4), suggesting decomposition of other forms of $CaCO_3$ (non amorphous). It is believed that this peak is related to the decomposition of calcite, as low crystalline calcite with high dispersity is thermally less stable and preferentially decomposes within the temperature range of 680-775°C [39].

Generally, the amount of carbonates increases with GBFS in the pastes, but still alkali-activated pastes have lower carbonate amounts compared to pastes CEM I and CEM III/B (Table 4, QXRD results). As for carbonate phases in cement-based pastes, higher proportion of vaterite in paste CEM I than in paste CEM III/B is believed to be a consequence of initially higher portlandite content in paste CEM I and due to similarities in the portlandite and vaterite symmetries [40] and their (positive) surface charge [41] as already observed by Black et al. [35].

In order to compare the tendencies of pastes to bind the $CO_2$, quantification of $CO_2$ uptake was done with two analyses, TG-DTG-MS and QXRD. Quantitative phase analysis by Rietveld method gives the $CO_2$ that is bound in the crystalline phases only. It can be seen that the largest portion of well crystallized carbonates is found for cement-based pastes. Regarding the disagreement between values for $CO_2$ uptake measured with TG-DTG-MS and QXRD (Table 4), it is clear that the TG-DTG-MS gives the highest values for $CO_2$ uptake because

$CO_2$ is contained in crystalline and amorphous carbonate phases, the latter not considered in XRD. The TG-DTG-MS values are also supported by FT-IR characterization of the early carbonation of the pastes, where it was evidenced that initially amorphous carbonates were formed. These metastable carbonates under the accelerated carbonation conditions were gradually converted into the more stable aragonite. However, not all the metastable carbonates were completely converted as shown by TG-DTG-MS results (Fig. 4).

The difference between the $CO_2$ uptake values measured with TG-DTG-MS and QXRD at 180 days, gives the amount of the $CO_2$ which is in amorphous form. The $CO_2$ binding capacity can be calculated from the chemical composition of the paste based on the (earth) alkaline content of each paste and assuming the stoichiometry of bonding (namely $CaO\text{-}CO_2$, $MgO\text{-}CO_2$, $NaOH\text{-}CO_2$, $KOH\text{-}CO_2$). Based on the calculated $CO_2$ binding capacities for the pastes (Table 4), the actual amount of $CO_2$ bound (TG-DTG-MS) was found to be less than the theoretical in all alkali-activated pastes.

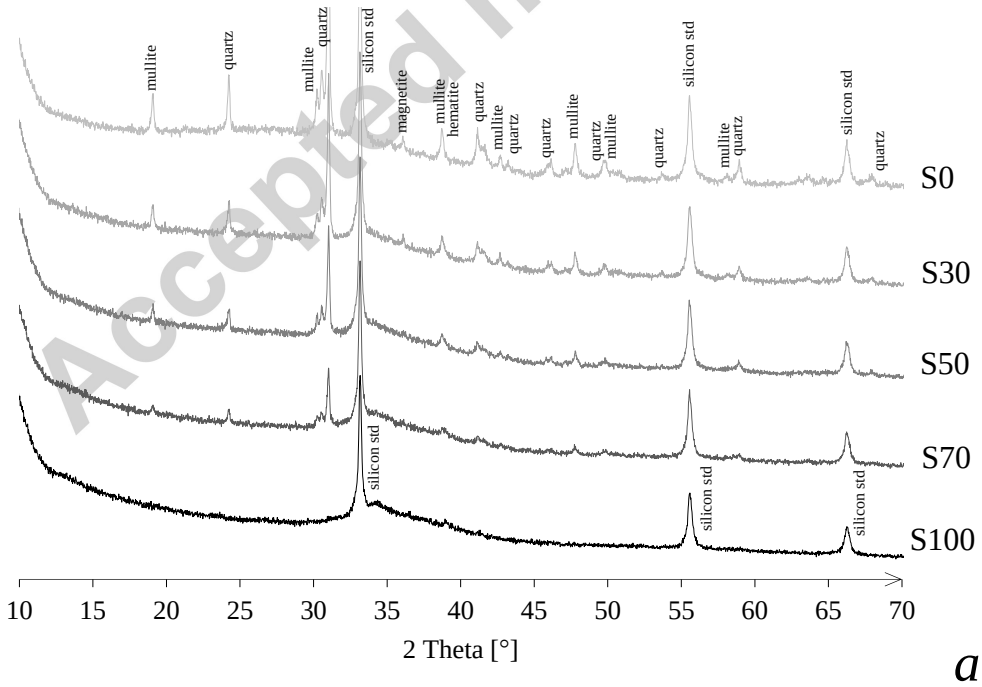


*a*

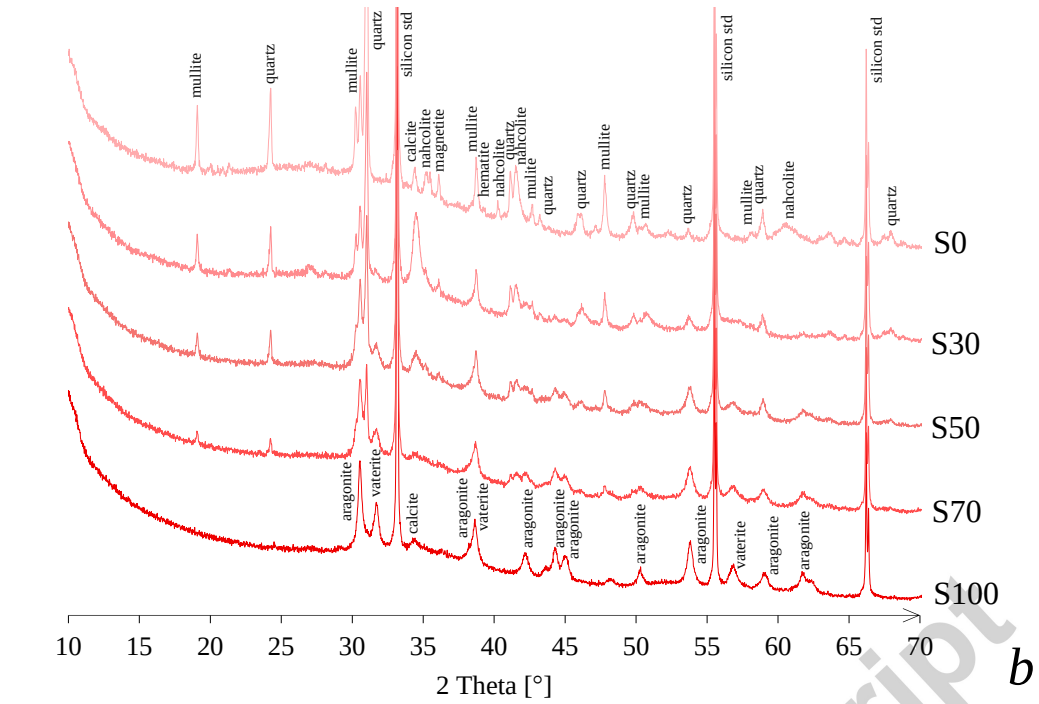


**Fig. 8.** XRD diffractograms with respect to the phases in alkali-activated FA and GBFS reference noncarbonated powders (*a*), and carbonated powders (*b*) after 180 days carbonation.

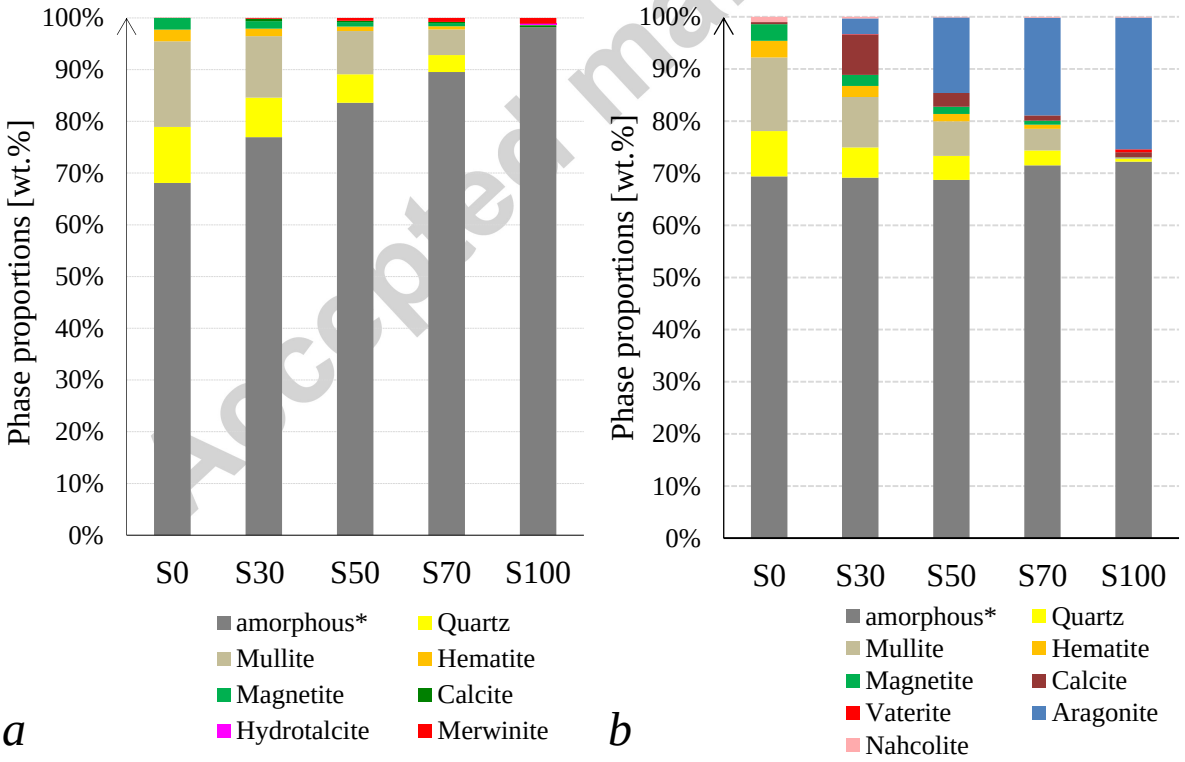


**Fig. 9.** Quantitative phase analysis by Rietveld method for (*a*) alkali-activated FA and GBFS reference noncarbonated powders, and carbonated powders (*b)* after 180 days carbonation.

**Table 4** The measured $CO_2$ uptake compared to the theoretical $CO_2$ uptake.

| | $CO_2$ uptake | | |
|---|---|---|---|
| | Theoretical[a] | QXRD[b] (180 days) | TG-DTG-MS[c] (180 days) |
| | [wt.%] | [wt.%] | [wt.%] |
| S0 | 14.85 | 0.70 | 5.30 |
| S30 | 24.74 | 5.04 | 14.68 |
| S50 | 30.87 | 7.66 | 16.09 |
| S70 | 37.32 | 8.82 | 15.00 |
| S100 | 47.81 | 11.88 | 14.36 |
| CEM III/B | 42.95 | 12.32 | 26.87 |
| CEM I | 51.15 | 17.16 | 35.95 |

[a]The theoretical $CO_2$ uptake is the sum of the individual (earth) alkaline oxide $CO_2$ binding capacities (the amount of $CO_2$ bound as $CaCO_3$, $MgCO_3$, $NaHCO_3$, $KHCO_3$), calculated as shown in equation {$\%CO_2 = 0.785(\%CaO - 0.56\%CaCO_3 - 0.7\%SO_3) + 1.091\%MgO + 1.42\%Na_2O + 0.94\%K_2O$} of Steinour [42]. The weight percent of oxides [%] was used from Table 1. It should be noted that $Na_2O$ weight was accounted from both the raw material and the alkaline activator for the calculation of the theoretical $CO_2$ uptake in alkali activated pastes.

[b]$CO_2$ uptake from the quantitative phase analysis by Rietveld method for paste carbonated powders after 180 days of carbonation (Fig.7 and Fig. 9), i.e. the amount of $CO_2$ bound as crystalline $CaCO_3$ and $NaHCO_3$, which were detected from the XRD analysis.

[c]$CO_2$ uptake from Fig. 4, quantified with TG-DTG-MS method from the powders after 180 days of carbonation, i.e. the amount of $CO_2$ bound as amorphous and crystalline $CaCO_3$ and $NaHCO_3$, which were detected from the TG-DTG-MS analysis.

**Table 5** Quantitative phase analysis with Rietveld method for reference pastes and for the carbonated crushed pastes.

| Phases | Amorphous | Quartz | Mullite | Magnetite | Hematite | Hydrotalcite | Vaterite | Aragonite | Calcite | Natron | Nahcolite |
|---|---|---|---|---|---|---|---|---|---|---|---|
| Reference | | | | | Sealed paste samples (No $CO_2$) | | | | | | |
| S0 | 75.2 | 8.6 | 12.7 | 2.3 | 0.6 | | | | 0.6 | | |
| S30 | 82.8 | 5.9 | 8.7 | 1.6 | 0.6 | | 0.1 | | 0.3 | | |
| S50 | 91.7 | 3.0 | 4.2 | 0.8 | 0.2 | | | | 0.1 | | |
| S70 | 94.1 | 2.1 | 3.1 | 0.4 | 0.1 | | | | 0.2 | | |
| S100 | 99.8 | 0.0 | 0.0 | 0.0 | 0.0 | | | | 0.2 | | |
| Accelerated | | | | | Carbonated crushed pastes | | | | | | |
| S0 | 71.1 | 8.9 | 14.5 | 3.3 | 0.8 | | | 0.0 | 0.4 | | 1.0 |
| S30 | 70.1 | 5.9 | 9.8 | 2.1 | 0.7 | | 0.1 | 3.2 | 7.8 | | 0.3 |
| S50 | 69.3 | 4.7 | 6.7 | 1.4 | 0.5 | | | 14.6 | 2.7 | | 0.1 |
| S70 | 71.9 | 2.9 | 4.2 | 0.8 | 0.2 | | | 18.8 | 1.0 | | 0.2 |
| S100 | 72.2 | 0.5 | 0.2 | 0.0 | 0.1 | | 0.6 | 25.3 | 1.0 | | 0.1 |

### 3.4 Implications for $CO_2$ uptake by alkali-activated pastes

Carbonation is the most common reason of the concrete deterioration under environmental conditions [8]. It induces chemical and physical changes to the cement paste properties that further influence its long-term performance. In this paper the $CO_2$ binding capacity, carbonate phases and the dynamic of gel changes under accelerated carbonation have been studied in both cement pastes and blended FA-GBFS alkali-activated pastes.

The results showed that with increase of the GBFS content in alkali activated pastes, the proportion of crystalline carbonates increases. In addition, while calcite decreases, aragonite increases. For all alkali activated pastes (excluding S0) the total amount of $CO_2$ bound after 180 days is almost the same. Crystalline Na-(bi)carbonates play a very minor to no role. Comparing this to the full carbonation potential as theoretically calculated, apparently lots of the (earth) alkalis are not available for carbonation in the alkali activated pastes. TG-DTG-MS results show a larger amount of these available (earth) alkalies are carbonated in FA-rich pastes (60% in S30) compared to GBFS-rich pastes (25% in S100).

In contrast to alkali activated pastes, cement-based pastes reach a much higher (equilibrium) carbonation level in well exposed grains. That is 63-70% of theoretical capacity of which 43-47% is in the form of crystalline carbonates and the rest is in amorphous form. This clearly indicates that there is a reduced potential for the $CO_2$ uptake to take place over the service life of alkali-activated materials compared to cement-based materials. Furthermore, FA-GBFS containing pastes show similar $CO_2$ binding capacity. Consequently, the increase of GBFS in the system did not contribute to higher $CO_2$ binding under accelerated carbonation conditions.

Modification of the amorphous aluminosilicate gel was also a result of carbonation. The aluminosilicate gel was characterised by a degree of polymerisation higher than the original C-S-H/C-N-A-S-H gel. Aluminosilicate gel may capture substantial Na in the structure as shown by the reactions (1-3), that does not allow formation of Na-carbonates. This is consistent with XRD results, where it was shown that Na-carbonates (nahcolite) content is too low and at the level of measurement error (Table 5).

The preservation of $OH^-$ and $Na^+$ ions in the pore solution or in the gel of the alkali activated pastes during carbonation would reduce the risk of pore solution neutralization which is important for preserving the passivity of the reinforcement oxide layer in alkali-activated concrete. However, the gel deterioration due to carbonation that leads to Ca leaching and polymerization of remaining aluminosilicate units certainly affects the overall microstructure and have negative effects on the micromechanical properties of the alkali-activated pastes as exemplified in [6].

## 4. Conclusions

The aim of this paper was to investigate the $CO_2$ binding capacity and mineralogical changes of alkali-activated and cement pastes under accelerated carbonation conditions. All the samples were cured for 28 days under sealed conditions before they were carbonated. To accelerate the process, the pastes were crushed and ground to powder. Based on the results presented in the paper, following conclusions can be drawn:

- Carbonation causes polymerization of the alumino-silicate network of the C-N-A-S-H gel in alkali activated FA-GBFS pastes. In cement-based pastes carbonation induces polymerization of C-S-H and loss of CH.
- With increase of the GBFS content in the pastes, the proportion of crystalline $CaCO_3$ increases, calcite decreases and aragonite increases.
- In all the alkali activated pastes studied here (excluding S0), the total amount of $CO_2$ bound after 180 days is similar. Crystalline Na-(bi)carbonates play a very minor to no role. Comparing this to the full carbonation potential as theoretically calculated, apparently lots of the (earth) alkalies are not available for carbonation in alkali activated pastes. The TG-DTG-MS results show that among the available alkalies, a large amount (60% in S30) is carbonated in FA-rich pastes compared to GBFS-rich pastes (25% in S100). In contrast to alkali activated pastes, cement-based pastes reach a much higher (equilibrium) carbonation level for well exposed grains of 63-70% of theoretical capacity of which 43-47% is in the form of crystalline carbonates and the rest is in amorphous form.
- Time-series FT-IR measurements showed that spectral changes related to the silicate polymerization of the decalcified gels were more significant in cement-based pastes.

This means that the microstructure of the aluminosilcate gel structure was more affected in the cement-based pastes than in the alkali activated pastes. These changes of silicate positions were predominant in the first 7 days. Although, the changes in carbonates continued up to 180 days. This shows that the transformation of carbonates from initially amorphous $CO_2$ to eventually crystalline compounds is a slow process that naturally occurs without any additional $CO_2$ uptake.

- Effect of the longer exposure time (28 vs 180 days) was shown, with TG-DTG-MS, to be significant for $CO_2$ uptake in cement-based and FA rich (S30) alkali activated pastes.



## Acknowledgement

This research was carried out under the project S81.1.13498 in the framework of the Partnership Program of the Materials innovation institute M2i (www.m2i.nl) and the Technology Foundation STW (www.stw.nl), which is part of the Netherlands Organisation for Scientific Research (www.nwo.nl). The first author thanks Damir Kralj from Ruđer Bošković Institute, Zagreb, Croatia, for providing valuable data regarding FT-IR spectra of the standard $CaCO_3$. The second author acknowledges the financial support of the European Union's Marie Curie Individual Fellowship program under REAgrant agreement No. 701531.

## References

[1] J.L. Provis, A. Palomo, C. Shi, Advances in understanding alkali-activated materials, Cem. Concr. Res. 78 (2015) 110-125.

[2] K. Arbi, M. Nedeljkovic, Y. Zuo, G. Ye, A Review on the Durability of Alkali-Activated Fly Ash/Slag Systems, Ind. Eng. Chem. Res. 2016. 55(19) (2016) 5439-5453.

[3] N.Li, N. Farzadnia, C. Shi, Microstructural changes in alkali-activated slag mortars induced by accelerated carbonation, Cem. Concr. Res. 100 (2017) 214-226.

[4] S.A. Bernal, R.M. de Gutierrez, J.L. Provis, V. Rose, Effect of silicate modulus and metakaolin incorporation on the carbonation of alkali silicate-activated slags, Cem. Concr. Res. 40(6) (2010) 898-907.

[5] S.A. Bernal, J.L. Provis, B. Walkley, R. San Nicolas, J.D. Gehman, D.G. Brice, A.R. Kilcullen, P. Duxson, J.S. van Deventer, Gel nanostructure in alkali-activated binders based on slag and fly ash, and effects of accelerated carbonation, Cem. Concr. Res. 53(0) (2013) 127-144.

[6] M. Nedeljković, B. Šavija, Y. Zuo, M. Luković, G. Ye, Effect of natural carbonation on the pore structure and elastic modulus of the alkali-activated fly ash and slag pastes, Constr. Build. Mater. 161 (2018) 687-704.

[7] J.H.M. Visser, Influence of the carbon dioxide concentration on the resistance to carbonation of concrete, Constr. Build. Mater. 67(Part A) (2014) 8-13.

[8] L. Bertolini, B. Elsener, P. Pedeferri, E. Redaelli, R.B. Polder, Carbonation-Induced Corrosion, in: Corrosion of Steel in Concrete: Prevention, Diagnosis, Repair, Second Edition, John Wiley & Sons, 2013, pp. 79-92.

[9] B. Johannesson, P. Utgenannt, Microstructural changes caused by carbonation of cement mortar, Cem. Concr. Res. 31(6) (2001) 925-931.

[10] A. Leemann, P. Nygaard, J. Kaufmann, R. Loser, Relation between carbonation resistance, mix design and exposure of mortar and concrete, Cem. Concr. Compos. 62 (2015) 33-43.

[11] Z. Shi, B. Lothenbach, M.R. Geiker, J. Kaufmann, A. Leemann, S. Ferreiro, J. Skibsted, Experimental studies and thermodynamic modeling of the carbonation of Portland cement, metakaolin and limestone mortars. Cem. Concr. Res. 88 (2016) 60-72.

[12] M. Nedeljković, B, Ghiassi, S. van der Laan, G. Ye, Effect of curing conditions on the pore solution and carbonation resistance of alkali-activated fly ash and slag paste, Cem. Concr. Res. 2018. Submitted.

[13] C.E. White, L.L. Daemen, M. Hartl, K. Page, Intrinsic differences in atomic ordering of calcium (alumino) silicate hydrates in conventional and alkali-activated cements, Cem. Concr. Res. 67 (2015) 66-73.

[14] Y. Ma, , G. Ye, J. Hu, Micro-mechanical properties of alkali-activated fly ash evaluated by nanoindentation, Constr. Build. Mater. 147 (2017) 407-416.

[15] R.J. Myers, S.A. Bernal, R. San Nicolas, J.L. Provis, Generalized structural description of calcium–sodium aluminosilicate hydrate gels: the cross-linked substituted tobermorite model, Langmuir, 29 (17) (2013) 5294-5306.

[16] M.B. Haha, B. Lothenbach, G. Le Saout, F. Winnefeld, Influence of slag chemistry on the hydration of alkali-activated blast-furnace slag - Part I: Effect of MgO, Cem. Concr. Res. 2011. 41(9) (2011) 955-963.

[17] M. Palacios, F. Puertas, Effect of Carbonation on Alkali-Activated Slag Paste, J. Am. Ceram. Soc. 89 (10) (2006) 3211-3221.

[18] F. Puertas, M. Palacios, T. Vázquez, Carbonation process of alkali-activated slag mortars, J. Mater. Sci. 41(10) (2006) 3071-3082.

[19] S.A. Bernal, R. San Nicolas, R.J. Myers, R.M. de Gutiérrez, F. Puertas, J.S. van Deventer, J.L. Provis, MgO content of slag controls phase evolution and structural changes induced by accelerated carbonation in alkali-activated binders, Cem. Concr. Res. 57(0) (2014) 33-43.

[20] S.A. Bernal, J.L. Provis, R.M. De Gutiérrez, J.S. van Deventer, Accelerated carbonation testing of alkali-activated slag/metakaolin blended concretes: effect of exposure conditions, Mater. Struct. (2014) 1-17.

[21] S.A. Bernal, R.M. de Gutiérrez, A.L. Pedraza, J.L. Provis, E.D. Rodriguez, S. Delvasto, Effect of binder content on the performance of alkali-activated slag concretes, Cem. Concr. Res. 41(1) (2011) 1-8.

[22] K. Scrivener, R. Snellings, B. Lothenbach, A practical guide to microstructural analysis of cementitious materials, 2016 Crc Press.

[23] D. Kralj, L. Brečević, A.E. Nielsen, Vaterite growth and dissolution in aqueous solution I. Kinetics of crystal growth, J. Cryst. Growth, 104 (4) (1990) 793-800.

[24] J. García Carmona, J. Gómez Morales, R. Rodríguez Clemente, Rhombohedral-scalenohedral calcite transition produced by adjusting the solution electrical conductivity in the system $Ca(OH)_2$–$CO_2$–$H_2O$, J. Colloid Interface Sci. 261(2) (2003) 434-440.

[25] T.F. Sevelsted, J. Skibsted, Carbonation of C–S–H and C–A–S–H samples studied by 13C, 27Al and 29Si MAS NMR spectroscopy, Cem. Concr. Res. 71 (2015) 56-65.

[26] R. Kondo, M. Daimon, T. Akiba, Mechanisms and kinetics on carbonation of hardened cement, in 5th International Symposium on Cement Chemistry. 1969: Tokyo, Japan. pp. 402–409.

[27] F.A. Andersen, D. Kralj, Determination of the composition of calcite-vaterite mixtures by infrared spectrophotometry, Appl. Spectrosc. 45(10) (1991) 1748-1751.

[28] P. Yu, R.J. Kirkpatrick, B. Poe, P.F. McMillan, X. Cong, Structure of calcium silicate hydrate (C-S-H): Near-, Mid-, and Far-infrared spectroscopy, J. Am. Ceram. Soc. 82(3) (1999) 742-748.

[29] D. Dimas, I. Giannopoulou, D. Panias, Polymerization in sodium silicate solutions: a fundamental process in geopolymerization technology, J. Mater. Sci. 44(14) (2009) 3719-3730.

[30] W. Lee, J. van Deventer, Structural reorganisation of class F fly ash in alkaline silicate solutions, Colloids Surf., A, 211(1) (2002) 49-66.

[31] D.J. Anstice, C.L. Page, M.M. Page, The pore solution phase of carbonated cement pastes, Cem. Concr. Res. 35 (2) (2005) 377-383.

[32] M. Yousuf, A. Mollah, T.R. Hess, Y.N. Tsai, D.L. Cocke, An FTIR and XPS investigations of the effects of carbonation on the solidification/stabilization of cement based systems-Portland type V with zinc, Cem. Concr. Res. 23 (4) (1993) 773-784.

[33] M. Castellote, L. Fernandez, C. Andrade, C. Alonso, Chemical changes and phase analysis of OPC pastes carbonated at different $CO_2$ concentrations, Mater. Struct. 42(4) (2009) 515-525.

[34] E. Reardon, B. James, J. Abouchar, High pressure carbonation of cementitious grout, Cem. Concr. Res. 19(3) (1989) 385-399.

[35] L. Black, C. Breen, J. Yarwood, K. Garbev, P. Stemmermann, B. Gasharova, Structural features of C–S–H (I) and its carbonation in air—a Raman spectroscopic study. Part II: carbonated phases, J. Am. Ceram. Soc. 90(3) (2007) 908-917.

[36] N. Rafai, R. Letolle, P. Blanc, A. Person, P. Gegout, Isotope geochemistry (13C, 18O) of carbonation processes in concretes, Cem. Concr. Res. 21(2-3) (1991) 368-377.

[37] D.Chakraborty, S.K. Bhatia, Formation and aggregation of polymorphs in continuous precipitation. 2. Kinetics of $CaCO_3$ precipitation, Ind. Eng. Chem. Res. 35(6) (1996) 1995-2006.

[38] F.A. Andersen, L. Brecevic, Infrared spectra of amorphous and crystalline calcium carbonate, Acta Chem. Scand, 45(10) (1991) 1018-1024.

[39] M. Thiery, G. Villain, P. Dangla, G. Platret, Investigation of the carbonation front shape on cementitious materials: Effects of the chemical kinetics, Cem. Concr. Res. 37 (7) (2007) 1047-1058.

[40] J. McConnell, Vaterite from Ballycraigy, Lame, Northern Ireland, Mineral. Mag. 32 (1960) 534-544.

[41] K. Sawada, The mechanisms of crystallization and transformation of calcium carbonates, Pure Appl. Chem. 69(5) (1997) 921-928.

[42] H.H. Steinour, Some effects of carbon dioxide on mortars and concrete-discussion, J. Am. Concr. Inst. 30(2) (1959) 905-907.